A&A 641, A141 (2020)
https://doi.org/10.1051/0004-6361/202038606

Astronomy & Astrophysics

GALACTICNUCLEUS: A high angular-resolution JHK_s imaging survey of the Galactic centre

III. Evidence for wavelength-dependence of the extinction curve in the near-infrared

F. Nogueras-Lara[1], R. Schödel[2], N. Neumayer[1], E. Gallego-Cano[2,3], B. Shahzamanian[2], A. T. Gallego-Calvente[2], and F. Najarro[4]

[1] Max-Planck Institute for Astronomy, Königstuhl 17, 69117 Heidelberg, Germany
e-mail: nogueras@mpia.de
[2] Instituto de Astrofísica de Andalucía (IAA-CSIC), Glorieta de la Astronomía s/n, 18008 Granada, Spain
[3] Centro Astronómico Hispano-Alemán (CSIC-MPG), Observatorio Astronómico de Calar Alto, Sierra de los Filabres, 04550 Gérgal, Almería, Spain
[4] Centro de Astrobiología (CSIC/INTA), ctra. de Ajalvir km. 4, 28850 Torrejón de Ardoz, Madrid, Spain

Received 8 June 2020 / Accepted 6 July 2020

ABSTRACT

Context. The characterisation of the extinction curve in the near-infrared (NIR) is fundamental to analysing the structure and stellar population of the Galactic centre (GC), whose analysis is hampered by the extreme interstellar extinction ($A_V \sim 30$ mag) that varies on arc-second scales. Recent studies indicate that the behaviour of the extinction curve might be more complex than previously assumed, pointing towards a variation of the extinction curve as a function of wavelength.
Aims. We aim to analyse the variations of the extinction index, α, with wavelength, line-of-sight, and absolute extinction, extending previous analyses to a larger area of the innermost regions of the Galaxy.
Methods. We analysed the whole GALACTICNUCLEUS survey, a high-angular resolution (~0.2″) JHK_s NIR survey specially designed to observe the GC in unprecedented detail. It covers a region of ~6000 pc^2, comprising fields in the nuclear stellar disc, the inner bulge, and the transition region between them. We applied two independent methods based on red clump (RC) stars to constrain the extinction curve and analysed its variation superseding previous studies.
Results. We used more than 165 000 RC stars and increased the size of the regions analysed significantly to confirm that the extinction curve varies with the wavelength. We estimated a difference $\Delta\alpha = 0.21 \pm 0.07$ between the obtained extinction indices, $\alpha_{JH} = 2.44 \pm 0.05$ and $\alpha_{HK_s} = 2.23 \pm 0.05$. We also concluded that there is no significant variation of the extinction curve with wavelength, with the line-of-sight or the absolute extinction. Finally, we computed the ratios between extinctions, $A_J/A_H = 1.87 \pm 0.03$ and $A_H/A_{K_s} = 1.84 \pm 0.03$, consistent with all the regions of the GALACTICNUCLEUS catalogue.

Key words. Galaxy: center – Galaxy: bulge – Galaxy: structure – stars: horizontal-branch – dust, extinction

1. Introduction

The centre of the Milky Way is the closest observable galactic nucleus and the only one we can look to in atttempting to resolve individual stars down to milli-parsec scales. It is, therefore, a unique laboratory to study the stellar nuclei and their role in the context of galaxy evolution. The Galactic centre (GC) is roughly delimited by the disc-like structure of the nuclear stellar disc (NSD) and the central molecular zone (e.g. Morris & Serabyn 1996; Launhardt et al. 2002; Kruijssen et al. 2014; Nogueras-Lara et al. 2020). It hosts a supermassive black hole, Sgr A*, in its dynamical centre that is embedded in a nuclear star cluster (e.g. Schödel et al. 2014; Neumayer et al. 2020).

The observation of the GC is hampered by the high stellar crowding and the extreme interstellar extinction ($A_V \gtrsim 30$ mag, $A_{K_s} \gtrsim 2.5$ mag, (e.g. Nishiyama et al. 2008; Schödel et al. 2010; Nogueras-Lara et al. 2018a) that limits the stellar analysis to near- and mid-infrared observations. In this sense, the GALACTICNUCLEUS survey (Nogueras-Lara et al. 2018a, 2019a) constitutes the most complete high-angular resolution (~0.2″) catalogue available to properly characterise the stellar population in the GC. This is a near infrared (NIR) multi-wavelength (JHK_s) survey that covers a total area of ~0.3 square degrees (~6000 pc^2) along the NSD, the inner bulge, and the transition regions between the inner bulge and the NSD (see Fig. 1).

The characterisation of the extinction curve in the NIR is fundamental for fully exploiting this data set and to be able to determine the structure and the stellar population of the innermost region of our Galaxy. Up to now, it has been widely accepted that it behaves like a power-law, $A_\lambda \propto \lambda^{-\alpha}$ (e.g. Nishiyama et al. 2008; Fritz et al. 2011), where λ is the wavelength and α is the extinction index. Nevertheless, recent studies have found some evidence of a wavelength-dependence of the extinction index (Nogueras-Lara et al. 2018a; Hosek et al. 2018). In particular, Nogueras-Lara et al. (2019b) analysed the extinction law in the NIR towards the central region of the NSD and found that the extinction index depends on wavelength, but not on the line-of-sight. This dependence has strong implications on the derivation

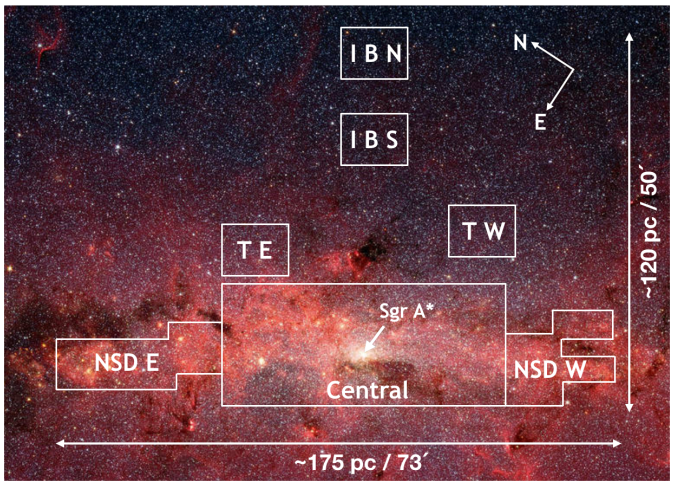

Fig. 1. Scheme of the GALACTICNUCLEUS survey over-plotted on a false colour *Spitzer*/IRAC image at 3.6, 4.5, 5.8, and 8 μm (credits: NASA/JPL-Caltech/S. Stolovy (*Spitzer* Science Center/Caltech)). Each of the regions are indicated in the figure: Central, NSD East (NSD E), NSD West (NSD W), transition East (T E), transition West (T W), inner bulge South (I B S), and inner bulge North (I B N).

of the structure of the innermost part of the Galaxy and the identification of the stellar type via NIR photometry, since a small change in the extinction index (∼10−15%) leads to a significant change in absolute extinction (∼0.3 mag, e.g. Matsunaga et al. 2016; Nogueras-Lara et al. 2019b) that might be translated into a biased estimation of the distance.

On the other hand, the study of the extinction curve using broadband filters is complex and requires the definition of a flux-weighted wavelength, known as effective wavelength ($\lambda_{\rm eff}$, e.g. Tokunaga & Vacca 2005). This quantity is not constant for a given filter and mainly depends on the absolute extinction and the spectral type of each star. The stellar metallicity, log$g$, and the atmospheric transmission also affect the value of $\lambda_{\rm eff}$, but to a lesser extent (see Tables B.1 and B.2 in Nogueras-Lara et al. 2018a). The necessary use of the effective wavelength hampers the analysis of the extinction curve, introducing degeneracies between different stellar types and the absolute value of extinction (for further details, see the appendix in Nogueras-Lara et al. 2018a). Namely, it is necessary to compute $\lambda_{\rm eff}$ independently for each individual star to characterise the extinction curve. This requires a knowledge of the spectral type of each star before computing the extinction indices, which is impossible given the high degeneracy existing between differential extinction and stellar types in the NIR (e.g. Nogueras-Lara et al. 2018a). To circumvent this problem, we use red clump stars (RC). They are red giants in their helium core-burning sequence (e.g. Girardi 2016) whose properties are well defined. They are abundant everywhere in the studied region and can be easily identified in the colour-magnitude diagrams (CMDs) using the NIR broadband filters, JHK_s (see Fig. 2).

In addition, the high level of differential extinction in the GC increases the complexity of the problem. We estimated that a variation in extinction of $\Delta K_s \sim 1$ mag (GC differential extinction estimated from Fig. 2) produces a change of the effective wavelength of RC stars of ∼0.5% for $\lambda_{\rm eff\_J}$ and $\lambda_{\rm eff\_K_s}$, and ∼1% for $\lambda_{\rm eff\_H}$. These variations are apparently small, but result in differences of 0.05–0.13 for the estimated values of the extinction indices. This change leads to an erroneous correction of the extinction, which makes the estimation of distance moduli or of stellar types from dereddening very difficult (for further details see Figs. 33 and 34 of Nogueras-Lara et al. 2018a). In this way, the uncertainties can be minimised by using RC stars and estimating the mean extinction towards regions of relatively small size.

In this work, we analyse, in detail, the extinction curve towards the GC using JHK_s photometry from the GALACTICNUCLEUS catalogue. We follow up the study initiated by Nogueras-Lara et al. (2019b) and extend it to the whole survey (∼6000 pc^2) by increasing the analysed area by a factor of four. Our study includes regions that belong to the GC and the inner bulge of the Galaxy.

2. Data

This work makes use of the GALACTICNUCLEUS survey (Nogueras-Lara et al. 2018a, 2019a) carried out using the HAWK-I camera (Kissler-Patig et al. 2008) at the ESO VLT unit telescope 4, which includes accurate JHK_s photometry of more than 3.3 million stars located in the GC and inner regions of the Galactic bulge. Figure 1 shows the fields included in the GALACTICNUCLEUS survey: three different regions distributed along the GC (Central, NSD East, and NSD West), two regions in the inner Galactic bulge (inner bulge South and inner bulge North), and two transition regions (transition East and West). The photometry was measured with the *StarFinder* software (Diolaiti et al. 2000) that performs the point spread function fitting and is optimised for crowded fields. The zero point (ZP) was calibrated using the SIRIUS IRSF survey (e.g. Nagayama et al. 2003; Nishiyama et al. 2006) and has a systematic uncertainty of 0.04 mag for all three bands. The photometry reaches 5 σ detections for $J \sim 22$, $H \sim 21$, and $K_s \sim 21$ mag. The statistical uncertainties are below 0.05 mag at $J \lesssim 21$, $H \lesssim 19$, and $K_s \lesssim 18$ mag (Nogueras-Lara et al. 2019a). This allows us to properly cover RC stars (e.g. Girardi 2016) at the GC distance and extinction conditions. Figure 2 shows the colour-magnitude diagram K_s versus $J - K_s$ of all the regions covered by the GALACTICNUCLEUS survey. The blue dashed parallelogram indicates the RC feature in each of the panels.

3. Extinction index variability with the wavelength

We used two different methods to compute the extinction indices between JH and HK_s.

3.1. Slopes of the RC feature

The slope of the RC feature in the CMDs indicates the direction of the reddening vector and can be used to compute the extinction index following Eq. (1) in Nogueras-Lara et al. (2018b, 2019b):

$$\alpha = -\frac{\log\left(1+\frac{1}{m}\right)}{\log\left(\frac{\lambda_{\rm eff_1}}{\lambda_{\rm eff_2}}\right)}, \quad (1)$$

where α is the extinction index, $\lambda_{\rm eff_1}$ and $\lambda_{\rm eff_2}$ are the effective wavelengths of the considered bands, and m is the slope of the RC feature in the CMD.

To apply this method: (1) the differential extinction must be large enough to result in an RC feature extended enough to allow us a reliable measurement of its slope; (2) it is necessary to have some previous information about the star formation history (SFH) of the analysed region. In particular, the brightness

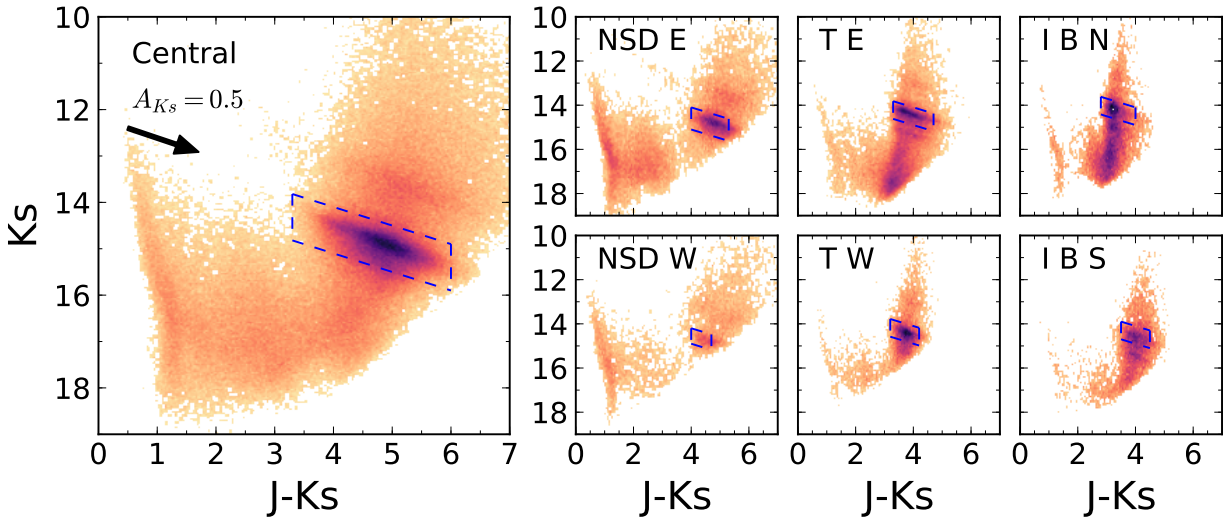

Fig. 2. Colour-magnitude diagrams K_s vs. $J - K_s$ of each of the regions observed by the GALACTICNUCLEUS survey: Central, NSD E, NSD W, TE, TW, IBN, and IBS correspond to the central region, the nuclear stellar disc East and West, the transition regions East and West, and the inner bulge North and South, as specified in Fig. 1. The blue dashed parallelograms indicate the position of the RC feature in each of the CMDs. The black arrow in the *left panel* depicts the reddening vector. The colour code indicates stellar densities, using a power stretch scale.

of RC stars depends on their ages, metallicity, and enhancement in alpha elements (e.g. Girardi 2016; Nogueras-Lara et al. 2018b). Moreover, a secondary clump formed by the red giant branch bump (RGBB) might also appear depending on the age and metallicity of the stellar population. Due to variations in the distance and line-of-sight extinction, the RC and RGBB features can be blended. Also, there can be degeneracies between the RGBB and a possibly fainter RC feature from a ∼1 Gyr old burst of star formation.

In the subsequent analysis, we only used the central region of the GALACTICNUCLEUS survey and the nuclear stellar disc East (NSD E, see Fig. 2). This is due to the required quality and the previous knowledge on the SFH (Nogueras-Lara et al. 2020). Moreover, it is only in these fields that the differential extinction is large enough to reliably measure the slope of the RC feature in the CMDs. We excluded the nuclear stellar disc West due to the bad quality of the data (too few stars detected caused by bad weather conditions). The transition regions (T E and T W) were not considered due to the mixture of populations between the inner bulge and the NSD that can affect the calculation of the slopes. We also excluded the inner bulge regions given the differential extinction in the K_s versus $H - K_s$ diagram is much smaller than in the central regions and this effect could lead to an incorrect estimation of the slopes.

Recent work on the NSD by Nogueras-Lara et al. (2020), points towards a mainly old stellar population (>80% of the mass older than 8 Gyr) and an important star-formation event ∼1 Gyr ago (>5% of the mass), implying a double RC sequence in the CMDs (see Fig. 1 of Nogueras-Lara et al. 2020). Nogueras-Lara et al. (2019b) analysed in detail the central ∼1700 pc^2 of the GALACTICNUCLEUS survey. Here, we increase the studied area by a factor of ∼2 and we also analyse the NSD E field.

We used all the stars in the RC features as shown by the blue dashed parallelograms in Fig. 3. The CMDs include stars belonging to several different pointings from the GALACTICNUCLEUS survey that were obtained under different observing conditions and different dates (see Tables A.1–A.3 in Nogueras-Lara et al. 2019a). Moreover, the differential extinction varies significantly across the observed field (Nogueras-Lara et al. 2018a, 2019b), which influences the position of the RC features

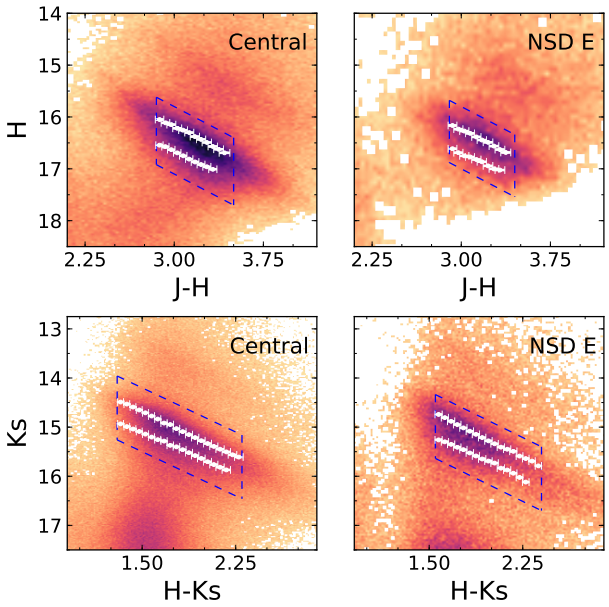

Fig. 3. Colour-magnitude diagrams H vs. $J - H$ of (*upper panels*), and K_s vs. $H - K_s$ (*lower panels*) for the central region of the GALACTICNUCLEUS survey (*left panels*), and the NSD East (*right panels*). The blue dashed parallelograms indicate the stars considered to compute the slope of the RC features. White dots depict the solutions obtained when applying the GMM method and their associated uncertainties.

in the CMDs depending on the line-of-sight. Thus, the selection of the RC is made in a way that the RC features present a homogeneous density in the CMDs and are not significantly affected by foreground population or low completeness. In this way, we excluded the bright part of the RC feature since it might contain stars belonging to the inner bulge (Nogueras-Lara et al. 2020) and the faint end since it is more affected by extinction and incompleteness.

To analyse the RC features and compute their slopes, we applied the methodology described in Sect. 3 of Nogueras-Lara et al. (2018b) and Sect. 4.4 of Nogueras-Lara et al. (2019b).

Table 1. Extinction index calculation following the method described in Sect. 3.1.

Extinction index	Central	NSD E
$\alpha_{JH\_\mathrm{bright}}$	$2.43 \pm 0.05 \pm 0.03$	$2.43 \pm 0.04 \pm 0.03$
$\alpha_{JH\_\mathrm{faint}}$	$2.53 \pm 0.05 \pm 0.06$	$2.61 \pm 0.10 \pm 0.09$
$\alpha_{JH\_\mathrm{average}}$	$2.48 \pm 0.04 \pm 0.03$	$2.52 \pm 0.05 \pm 0.05$
$\alpha_{HK_s\_\mathrm{bright}}$	$2.21 \pm 0.01 \pm 0.02$	$2.13 \pm 0.02 \pm 0.01$
$\alpha_{HK_s\_\mathrm{faint}}$	$2.36 \pm 0.01 \pm 0.03$	$2.23 \pm 0.05 \pm 0.03$
$\alpha_{HK_s\_\mathrm{average}}$	$2.29 \pm 0.01 \pm 0.02$	$2.18 \pm 0.03 \pm 0.02$

Notes. The uncertainties correspond to the statistical and systematic ones, respectively.

Namely, we divided the RC regions into small vertical bins of 0.05 mag width and confirmed that they correspond to a double RC sequence. For this purpose, we considered each vertical bin and fitted the underlying K_s-band distribution with a one-Gaussian model and a two-Gaussians one, applying the SCIKIT-LEARN python function GaussianMixture (GMM, Pedregosa et al. 2011). We obtained that a two-Gaussians model fits the data better in all cases, using the Bayesian information criterion (Schwarz 1978) and the Akaike information criterion (Akaike 1974), as expected given the SFH of the analysed regions. To compute the slope of the features, we used a jackknife algorithm considering the values obtained from the two-Gaussians fits and the median colours of the vertical bins (see Fig. 3). The slopes were obtained as the mean of the re-sampling data sets in the jackknife algorithm and the associated uncertainties were estimated as their variances. We calculated the extinction indices using Eq. (1) (see Table 1). The effective wavelengths were computed following the Eq. (A.3) of Tokunaga & Vacca (2005), as explained in Appendix B of Nogueras-Lara et al. (2018a), using an index of 2.30 ± 0.08 (Nogueras-Lara et al. 2018a) and the $A_{1.61}$ values shown in Table 2.

Table 1 shows the results, where the statistical and systematic uncertainties are specified. The statistical uncertainties were estimated considering the uncertainties of the slopes and the effective wavelengths (see Appendix B of Nogueras-Lara et al. 2018a). To obtain the systematics, we varied the width and the number of vertical bins (implying different cuts at the faint end) and the selection box of the RC stars (blue dashed parallelograms in Fig. 3). In all cases, we removed the faint red end of the secondary RC feature to avoid problems related to the greater incompleteness of this feature (Nogueras-Lara et al. 2019b). The extinction indices obtained using the faint features are somewhat larger than the ones obtained by means of the bright one. We believe that the reason may be that the secondary RC is fainter and has a significantly lower number of stars than the bright one. Therefore, it is significantly more affected by incompleteness, differential extinction, and the presence of recent star formation. In this way, we calculated the extinction indices combining the obtained values for both features to account for possible systematic effects. Table 1 shows the average values and their associated uncertainties.

3.1.1. Wavelength variability

Comparing the extinction indices computed previously for JH and HK_s ($\Delta\alpha = \alpha_{JH} - \alpha_{HK_s}$), we obtained $\Delta\alpha_{\mathrm{central}} = 0.19 \pm 0.05$ and $\Delta\alpha_{\mathrm{NSD\ E}} = 0.34 \pm 0.06$, where the statistical and systematic uncertainties of each α were propagated quadratically. Combining both measurements, we obtained $\Delta\alpha = 0.27 \pm 0.04$, where the uncertainty was computed propagating the uncertainty of each measurement. This implies that the difference in the extinction indices is detected with $\gtrsim 6\,\sigma$ significance.

3.1.2. Completeness effect

We also analysed the effect of completeness on our results. Given the high number of sources in our fields, the standard approach of inserting and recovering artificial stars is not feasible due to enormous amount of computational time required. Instead, we used an alternative approach computing the critical distance at which a star of any magnitude might be detected around a given brighter star (Eisenhauer et al. 1998). This allows us to account for completeness due to crowding, which dominates the incompleteness in the highly crowded regions studied (Nogueras-Lara et al. 2020). We considered the central region of the GALACTICNUCLEUS survey as a test case. This is because this is the most crowded region of the survey and the effect of incompleteness due to crowding will be maximum here. Thus, if there is some influence of incompleteness on our results, it will be easily identified in this region. Since this method assumes that the probability of detecting a source with a given magnitude is uniform within the field, we divided the region into small sub-regions of $2' \times 1.4'$. We averaged over the completeness solutions obtained for each sub-region to get the final one (for further details, see Nogueras-Lara et al. 2020). We ended up with an 80% of completeness level for $J \sim 18.4$ mag, $H \sim 18.3$ mag, and $K_s \sim 16.3$ mag. Nevertheless, the completeness for J band (and presumably H band as well) is probably overestimated since the crowding becomes the limiting factor for longer wavelengths (i.e. K_s band). This is attributed to two main causes: (1) the shorter the wavelength, the more important is the extinction effect and less stars are detected. Thus, the incompleteness due to the lack of sensitivity is significant and the crowding effect is less important. (2) The luminosity function is very similar to a power law outside of the RC (and at J band the differential extinction dilutes the RC extremely, so that a power law is a good approximation). Therefore, if the turnoff of the LF is at brighter magnitudes than the crowding completeness, then completeness is limited by sensitivity.

We corrected the CMDs for completeness by choosing a reference level with a completeness of 50% and randomly removing stars from the CMDs whose completeness is larger in order to normalise them to the reference level. For this, we computed the completeness levels on the CMDs H vs. $J - H$ and K_s vs. $H - K_s$ in steps of 1% to calculate the random fraction of stars to be removed in each 1% step. We generated 100 Monte Carlo samples of randomly removed stars and repeated the calculation of the extinction index using the bright RC feature of the CMDs, as previously explained. We obtained the standard deviation of the values as <0.01 for both α_{JH} and α_{HK_s}. Therefore, we concluded that the effect of completeness is negligible given the chosen selection of RC stars (blue parallelograms in Fig. 3).

We also checked the influence of completeness using different brightness cutoffs when computing the slopes of the features. We concluded that within the uncertainties and the selection of RC stars used here, there is no significant effect resulting from completeness on our results.

3.1.3. Effect of the nuclear star cluster

The central field of the GALACTICNUCLEUS survey includes the nuclear star cluster (NSC), whose SFH might be different in comparison to the NSD. In addition, the significantly higher

stellar density might result in a lower completeness of the data that might affect the RC features shown in Fig. 3. Namely, according to previous works, around 70–80% of the stars are older than 5 Gyr (Blum et al. 2003; Pfuhl et al. 2011). Therefore, the bright RC feature should not be significantly affected. Nevertheless, and as a sanity check, we repeated the analysis excluding all the stars within a radius of 5 pc (~2.2 arcmin) from Sgr A*, which corresponds to the effective radius of the NSC (e.g. Gallego-Cano et al. 2020). Using the bright RC feature, we obtained $\alpha_{JH} = 2.40 \pm 0.05 \pm 0.03$ and $\alpha_{HK_s} = 2.20 \pm 0.01 \pm 0.02$, which is in good agreement with the results that were previously obtained. Comparing the extinction indices, we computed $\Delta\alpha = 0.20 \pm 0.06$, where the uncertainties are added quadratically.

3.2. Model minimisation

We also analysed the extinction curve using RC stars and the "grid method" described in Nogueras-Lara et al. (2018a). This method assumes a Kurucz model (Kurucz 1993) for a RC star and generates a grid of extinction indices (α) and absolute extinctions ($A_{1.61}$) at a given wavelength ($\lambda = 1.61\,\mu$m). We made the grid finer with step sizes ~3 times smaller compared to previous works (step of 0.005 for α and $A_{1.61}$). Applying the grid, we reddened the synthetic model to be compared with the real data via χ^2 minimisation. The RC stellar model considers $T = 4750 \pm 250$ K, $\log g = +2.5$ (Bovy et al. 2014), a radius of $10.0 \pm 0.5\,R_\odot$ (e.g. Chaplin & Miglio 2013), and twice solar metallicity (e.g. Feldmeier-Krause et al. 2017; Schultheis et al. 2019; Nogueras-Lara et al. 2020). We assumed a distance to the GC of 8.0 ± 0.1 kpc, combining the results obtained by GRAVITY Collaboration (2018) and Do et al. (2019). To estimate the systematic uncertainties, we repeated the calculation of α and $A_{1.61}$, independently considering the uncertainties of each of the parameters described earlier (for further details see Nogueras-Lara et al. 2018a, 2019b). Given the high number of stars used and the small step size of the grid, the computational time to estimate the uncertainties is too high. Therefore, we randomly selected a sample of 5000 stars for each of the GALACTICNUCLEUS' regions (we selected all the stars for regions where the number of RC stars is lower than 5000) to compute the systematics. Moreover, we also considered the systematic uncertainty of the photometric zero point, repeating the calculation of α and $A_{1.61}$ adding and subtracting the ZP systematics to the photometry of each band independently (0.04 mag in all three bands, Nogueras-Lara et al. 2019a). The statistical uncertainties are not relevant in any case given the large number of stars used for the calculations.

We applied this method to the RC stars in the whole GALACTICNUCLEUS survey to study the variability of the extinction curve. Since we used only two bands to compute two unknowns (α and $A_{1.61}$), the grid method is similar to a geometric method in the CMD space, implying that it might be dependent on the stellar density of the selected RC features. Thus, to avoid selection effects, we used the CMD K_s vs. $J - K_s$ when analysing the extinction indices for JH and HK_s. The blue dashed parallelograms in Fig. 2 indicate the RC stars used for each region. This selection depends on the stellar density of the RC feature for each field. In this way, the RC feature is narrower for the transition and the inner bulge fields than in the regions belonging to the NSD. This is because for the RC, there are mainly old stellar populations and it does not have much contribution from stellar populations younger than 8 Gyr (Nogueras-Lara et al. 2018b, 2020). Moreover, we only used stars detected in all three bands and excluded the faint end of the RC feature to avoid regions with low completeness.

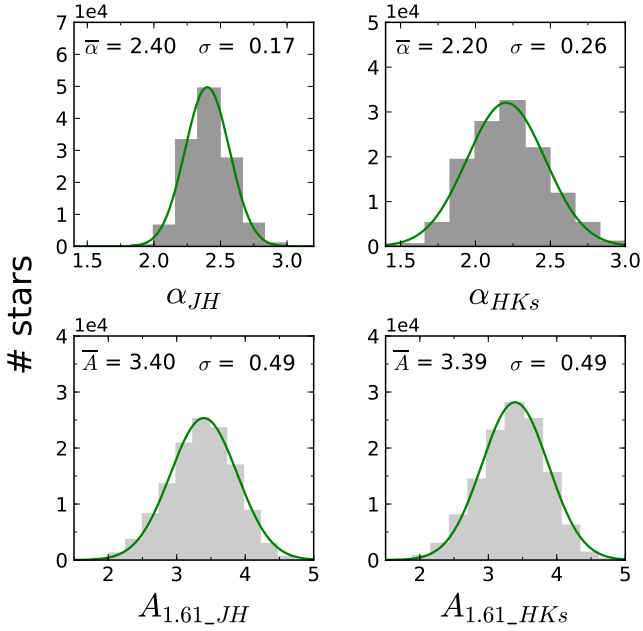

Fig. 4. Extinction indices (α_{JH} and α_{HK_s}) and absolute extinction ($A_{1.61\_JH}$ and $A_{1.61\_HK_s}$) distributions, *upper and lower panels*, respectively. The green line indicates a Gaussian fit whose mean and standard deviations are specified in each panel.

Figure 4 shows the obtained α and $A_{1.61}$ distributions for the central region of the GALACTICNUCLEUS survey as an example. Table 2 summarises the results obtained for each region in the catalogue. We found that the α_{HK_s} uncertainties are a factor ~2 larger than the ones for α_{JH}. This is because variations in the ZP, the distance to the stars, in addition to the temperature and radius of the RC stars affect the calculation of α_{HK_s} in a more significant way. On the other hand, to assess our results, we confirmed that the values of extinction, $A_{1.61\_JH}$ and $A_{1.61\_HK_s}$, obtained when computing the extinction indices using the bands JH and HK_s, are in agreement, as expected (Table 2).

3.2.1. Wavelength variability

We computed $\Delta\alpha$ for each region using the values obtained for α_{JH} and α_{HK_s}. We estimated the uncertainties by repeating the calculation of α_{JH} and α_{HK_s} considering the uncertainties of the parameters involved in their calculation. Again we used the approach of selecting a random sample of 5000 RC stars to avoid overly long computational time frames (see Sect. 3.2 for details). For each of the parameters, we calculated the uncertainty on $\Delta\alpha$ and propagated it quadratically. Since the variation of some of the parameters affects α_{JH} and α_{HK_s} in the same direction, the final uncertainty is lower than the obtained when propagating the individual uncertainties computed previously for each extinction index (Table 2). The H and K_s ZP systematics are the most important source of uncertainty for $\Delta\alpha$. The last column of Table 2 shows the results. We observed that the extinction indices, α_{JH} and α_{HK_s}, are different for all the regions analysed with ~2σ significance. Computing the $\Delta\alpha$ averaging over the values obtained for each of the regions, we ended up with a value of $\Delta\alpha = 0.21 \pm 0.06$, where the uncertainty refers to the standard deviation of the distribution of $\Delta\alpha$.

Table 2. Obtained values for α and $A_{1.61}$ using the grid method.

	α_{JH}	α_{HK}	$A_{1.61\_JH}$	$A_{1.61\_HK}$	$\Delta\alpha$
Central	2.40 ± 0.07	2.20 ± 0.12	3.40 ± 0.12	3.39 ± 0.12	0.20 ± 0.12
NSD E	2.42 ± 0.07	2.25 ± 0.12	3.29 ± 0.12	3.29 ± 0.12	0.17 ± 0.12
NSD W	2.38 ± 0.08	–	2.96 ± 0.12	–	–
T E	2.45 ± 0.09	2.32 ± 0.16	2.56 ± 0.12	2.56 ± 0.12	0.13 ± 0.15
T W	2.45 ± 0.10	2.21 ± 0.16	2.47 ± 0.12	2.47 ± 0.12	0.24 ± 0.15
I B S	2.40 ± 0.08	2.21 ± 0.15	2.71 ± 0.12	2.70 ± 0.12	0.19 ± 0.14
I B N	2.50 ± 0.11	2.17 ± 0.18	2.12 ± 0.12	2.11 ± 0.12	0.33 ± 0.17

Notes. $A_{1.61\_JH}$ and $A_{1.61\_HK}$ indicate the value of the extinction at 1.61 μm obtained using the bands JH and HK_s, respectively. The uncertainties correspond to the systematic ones. The statistical uncertainties are negligible given the high number of stars used for the calculation. The α_{HK} and $A_{1.61\_HK}$ values for the NSD W were not computed due to the low number of stars detected in the RC feature and the bad weather conditions when observing K_s band. It affected the photometry as indicated by the scattering in Fig. 7 of Nogueras-Lara et al. (2019a) and might lead to biased results.

3.2.2. Completeness effect

We also estimated the influence of completeness on our results. We considered the central region and followed the approach described previously (see Sect. 3.1.2). We computed the completeness solution for J and K_s since we used the CMD K_s vs. $J - K_s$ to select the RC stars. We generated 100 samples of randomly selected completeness corrected stellar lists and computed the extinction indices and $A_{1.61}$. Ultimately, there was no any significant change of the measured values of the results for α_{JH}, α_{HK_s}, A_{JH}, and A_{HK_s}. Therefore, we conclude that completeness does not affect our results in any significant way within the selected stellar sample.

4. The extinction index as a function of absolute extinction

We studied the variability of the extinction index with the absolute extinction with two different approaches.

4.1. Different GALACTICNUCLEUS regions

Using the grid method, we obtained α_{JH}, α_{HK_s}, $A_{1.61\_JH}$, and $A_{1.61\_HK_s}$ for six different regions of the GALACTICNUCLEUS survey (Table 2). Given that the mean extinction varies significantly between them, we analysed the variability of the extinction indices with the absolute extinction obtained for each of the regions. Figure 5 shows the result. We computed the uncertainties assuming that the only significant relative difference between the studied regions corresponds to the possible ZP systematics. We conclude that there is no significant dependence of the extinction indices (α_{JH} and α_{HK_s}) with the absolute extinction for the range of observed absolute extinctions within the obtained uncertainties. Computing the mean and the standard deviation of the six extinction indices, we ended up with $\alpha_{JH} = 2.44 \pm 0.03$ and $\alpha_{HK_s} = 2.23 \pm 0.05$.

4.2. Grid method for different cuts in the CMD

We also studied the variability of the extinction index with the absolute extinction within the same regions, computing α_{JH} and α_{HK_s} by using the grid method for different colour cuts in the CMD K_s vs. $J - K_s$ as done in Sect. 4.3 of Nogueras-Lara et al. (2019b). We found that α_{JH} is compatible with a constant extinction index, whereas α_{HK_s} shows some tendency to be larger at larger values of absolute extinction in the central, inner bulge South, and inner bulge North regions. Figure 6 shows the results. In particular, this difference is $\gtrsim$0.1 for α_{HK_s} in the central region of the GALACTICNUCLEUS survey for a variation in $A_{1.61} \sim 2$ mag. Nevertheless, this tendency does not appear for the nuclear stellar disk East and the transition regions of East and West. Moreover, the largest variations are observed for α_{HK_s} which is more sensitive to small changes in the parameters that affect the calculation (see Sect. 3.2). Therefore, we believe that this tendency is not real.

On the other hand, and, in particular, for the central region where the variation is largest, the presence of a different foreground population (old and alpha enhanced from the inner bulge, e.g. Nogueras-Lara et al. 2018b), might also explain slightly different values when computing the extinction index there. We concluded that the previously obtained mean values of $\alpha_{JH} = 2.44 \pm 0.03$ and $\alpha_{HK_s} = 2.23 \pm 0.05$ are more reliable and cover the observed variations of the extinction indices well within the uncertainties.

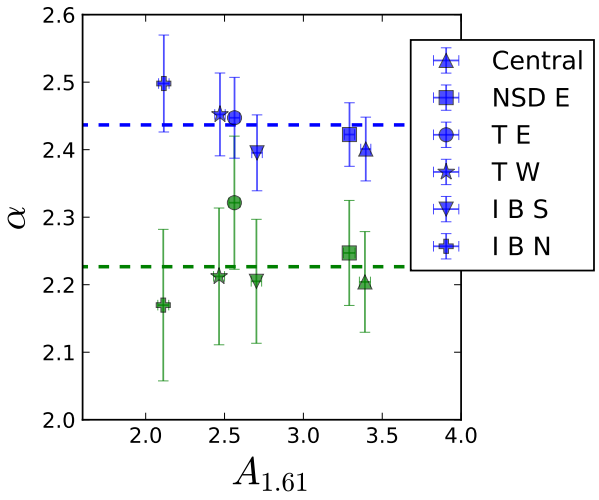

Fig. 5. Extinction index variability as a function of the absolute extinction ($A_{1.61}$). The upper blue and lower green points indicate α_{JH} and α_{HK_s}, respectively. The legend indicates the symbols corresponding to a given region of the GALACTICNUCLEUS survey. The uncertainties were computed considering the ZP systematics between regions. The green and blue dashed line indicate a flat profile to be compared with the extinction indices and their uncertainties.

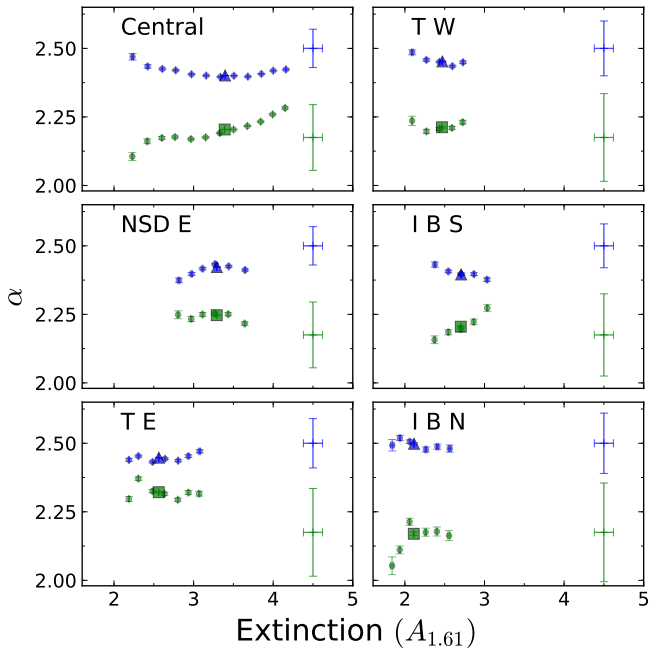

Fig. 6. Extinction index variability with the absolute extinction ($A_{1.61}$) for six different regions of the GALACTICNUCLEUS survey (indicated for each panel). The upper blue points and lower green ones indicate the values of α_{JH} and α_{HK_s} for each absolute extinction $A_{1.61}$, including the statistical uncertainties. Big blue triangles and green squares indicate the average value per region obtained in Table 2. The blue and green crosses indicate the systematic uncertainties due to the ZP computed for each region.

This approach of using colour cuts in the CMD K_s vs. $J - K_s$ has several limitations that might introduce the tendency observed for the central, inner bulge South, and inner bulge North regions (see Fig. 6):

- A vertical cut in the CMD K_s vs. $J - K_s$ introduces selection effects on the stars used to compute the extinction indices. Namely, the intrinsic scatter in the plot and the partial degeneracy between the extinction and the extinction index impede to select a clean sample of stars corresponding to a given extinction. The shorter the bins, the greater this effect. Furthermore, the distribution of the extinction indices for a given cut is not fully Gaussian due to this effect.
- The grid method using two bands to compute two unknowns (α and $A_{1.61}$) is similar to a geometric method in the CMD space and is dependent on the density of sources in the given RC feature. Therefore, cutting this feature into small bins introduces systematics effects that might produce a variation in the extinction index and absolute extinction with the number and density of RC stars for each bin.
- We need to know the distance to the RC stars to compute α and $A_{1.61}$. The distance to the GC is a good estimate if we average over all the stars, but slightly different distances might become significant when considering colour cuts in the CMD. Moreover, the transparency varies between different regions of the NSD due to the presence or not of dusty clouds. Therefore, the contribution from the NSD's edge may vary, slightly changing the average distance to the observed stars. We estimated that a change in ∼200 pc (∼ diameter of the NSD, e.g. Nishiyama et al. 2013; Gallego-Cano et al. 2020) can produce a variation of α_{HK_s} around 0.05. This effect is less important for α_{JH}, where it accounts for ∼0.02. This also applies to the previous effects and explains why we always observed a constant α_{JH} for all the analysed regions. The only way to reduce these effects is to select wide bins that contains a large number of stars in the RC feature, whose average distance is less biased, as we did in Sect. 3.2.

4.3. Effect on the RC feature in the CMD

We also tested whether the variation in the extinction index as a function of absolute extinction would produce any significant effect on the slope of the RC features in the CMD K_s vs. $H - K_s$. We assumed the α_{HK_s} vs. $A_{1.61}$ values obtained for the central region in Fig. 6 and computed the equivalent slope for each extinction bin, solving for m in Eq. (1). We reconstructed the distribution of points in the K_s vs. $H - K_s$ diagram following the changes of slope indicated by the m values. Finally, we computed the slope of all the computed points using a jackknife algorithm to estimate the uncertainties (see Sect. 3.1 for further details). We obtained that the points are well fitted by a linear fit with a slope of 1.219 ± 0.004. On the other hand, the slope computed for the bright RC feature of the central region in Sect. 3.1 was $1.217 \pm 0.010 \pm 0.015$, where the uncertainties refer to the statistical and the systematic ones, respectively. Therefore, given this variation in α_{HK}, the behaviour of the RC slope is not significantly affected, so it is not possible to detect whether there is some variation (of this scale) in the extinction index with absolute extinction using the slope of the RC feature.

5. Extinction index variability with the line of sight

Figure 5 informs also about the variability of the extinction indices α_{JH} and α_{HK_s} as a function of the line of sight. We studied six different regions in the GC that are separated a maximum distance of ∼0.6° (∼90 pc, see Fig. 1) and found that the extinction indices are compatible with being a constant of one within the uncertainties, as shown in the previous section.

We also studied the variability of the extinction indices at shorter spatial scales. For this, we analysed all the regions in the GALACTICNUCLEUS survey with the exception of the NSD West region which has a low data quality (see Sect. 3). We used the extinction indices obtained for individual RC stars with the grid method, as previously explained. We created extinction index maps dividing the analysed regions into a grid of pixels of 1.5 arcmin^2. We computed the values for each pixel using a $3\,\sigma$ clipping algorithm to reject outliers. We also excluded stars with photometric uncertainties larger than 0.05 mag in any single band and imposed a minimum number of 80 accepted stars to compute a pixel value (for further details, see Sect. 4.1. of Nogueras-Lara et al. 2019b). Figure 7 shows the maps obtained for α_{JH} and α_{HK_s}. We chose the same colour scale for both maps to highlight the wavelength dependence of the extinction index. We estimated the statistical uncertainties for each pixel by means of the error of the mean of the α distributions (standard deviation / (number of stars -1)$^{1/2}$). Considering the uncertainties for all the pixels, we obtained an average uncertainty of 0.01 for α_{JH}, and 0.02 for α_{HK_s}. The systematic uncertainties are irrelevant here because they affect all the values in the same direction. Nevertheless, since the GALACTICNUCLEUS survey is composed of 49 different pointings that were observed and photometrically calibrated in an independent way, the ZP systematics between different regions might cause a spurious variation. Considering the ZP systematic uncertainty of 0.04 for all the bands (Nogueras-Lara et al. 2019a), we estimated that the

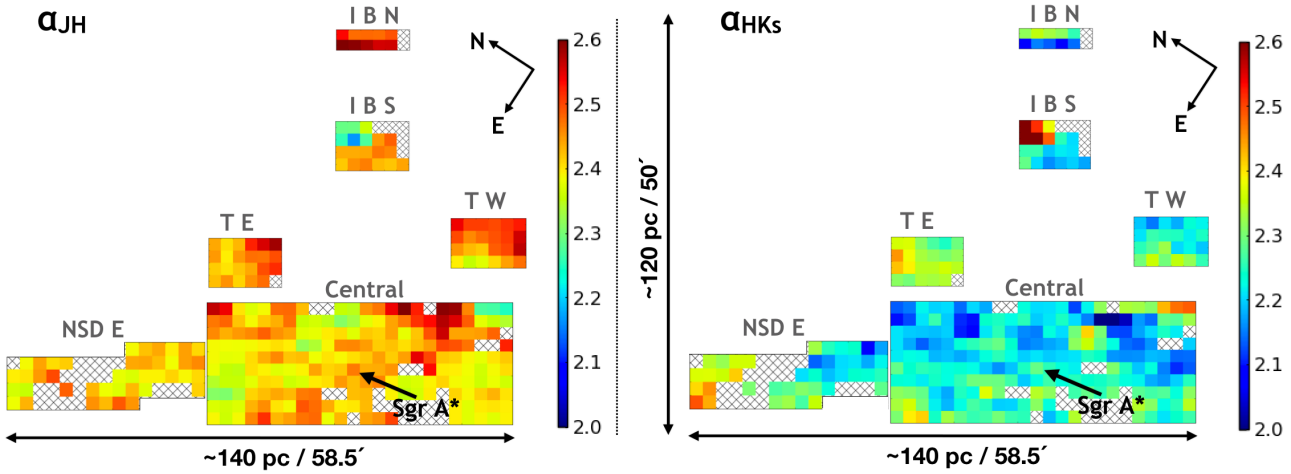

Fig. 7. Line-of-sight distribution of the extinction indices α_{JH} (*left panel*) and α_{HK_s} (*right panel*). Cross-shaped pixels indicate regions where the number of stars is not enough to compute a value for the extinction index. The labels specify the analysed regions of the GALACTICNUCLEUS survey. The scale of the colour bar is the same for both panels. The position of Sgr A* and the physical scales are shown in the figure.

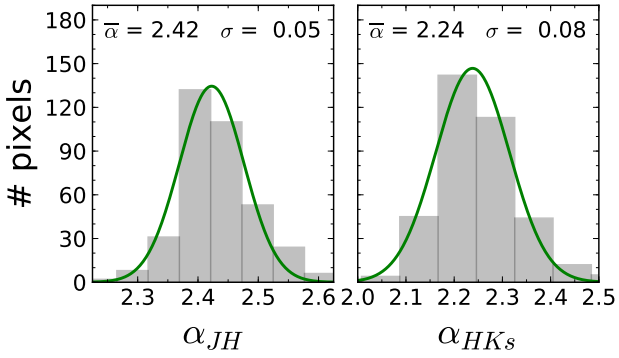

Fig. 8. Histograms of the extinction indices α_{JH} (*left panel*) and α_{HK_s} (*right panel*) per pixels using all the regions shown in Fig. 7. The green lines indicate a Gaussian fit whose mean and standard deviation values are specified on each panel.

extinction indices might vary by $\delta\alpha_{JH} \sim 0.05$ and $\delta\alpha_{HK_s} \sim 0.08$. Therefore, the previous effects are sufficient to justify the variations between pixels observed in Fig. 7. Moreover, some pixels that appear to be different from the surrounding ones, normally correspond to the shape of each HAWK-I pointing and show a correlation between α_{JH} and α_{HK_s}. This can be easily explained by a shift of the ZP for a given pointing in the H band, affecting both values, α_{JH} and α_{HK_s}.

To further analyse the constancy of the extinction indices with the line-of-sight, Fig. 8 shows the distribution of the α_{JH} and α_{HK_s} obtained for all the pixels. We found that the data properly follow a Gaussian distribution with mean values of $\alpha_{JH} = 2.42 \pm 0.05$ and $\alpha_{HK_s} = 2.24 \pm 0.08$, where the uncertainties correspond to the standard deviation. These uncertainties are perfectly compatible with the systematics due to the photometric zero point computed previously. Hence, our results point towards non-varying extinction indices with the line-of-sight within the uncertainties.

6. Final extinction index value

We analysed the extinction curve in the NIR towards the GC and found that the extinction index depends on the wavelength to a significant extent. On the other hand, it does not depend on the absolute extinction and on the line-of-sight within the estimated uncertainties. Next, we computed a final value for α_{JH} and α_{HK_s} by combining the values obtained for the different methods and regions that we used. We took the average values computed using the slopes of the RC features in Table 1 and all the individual values obtained using the grid method for the different regions of the GALACTICNUCLEUS survey (Table 2). We ended up with a mean value of $\alpha_{JH} = 2.44 \pm 0.05$ and $\alpha_{HK_s} = 2.23 \pm 0.05$, where the uncertainties were quadratically propagated.

We also computed the ratios between absolute extinctions, A_J/A_H and A_H/A_{K_s} using the following equation:

$$A_{\lambda_1}/A_{\lambda_2} = (\lambda_1/\lambda_2)^{-\alpha}, \quad (2)$$

where λ_i indicates effective wavelength, A_{λ_i} are the absolute extinctions for a given effective wavelength, and α is the corresponding extinction index. We computed the effective wavelengths considering the $A_{1.61}$ in Table 2 and obtained a consistent value of $A_J/A_H = 1.87 \pm 0.03$ and $A_H/A_{K_s} = 1.84 \pm 0.03$, where the uncertainties have been obtained quadratically propagating the associated uncertainties and considering the different values obtained using the different extinctions, $A_{1.61}$, associated to each of the regions of the GALACTICNUCLEUS survey.

7. Discussion and conclusion

In this paper, we analyse in detail the extinction curve towards the GC in the NIR by applying independent methods based on RC stars. For the first time, we used the whole GALACTICNUCLEUS survey (Nogueras-Lara et al. 2019a) and extended the study of the extinction to a large area of the NSD, the inner bulge, and the transition region between the GC and the inner bulge, covering a total area of ~6000 pc^2. For the analysis, we used more than 165 000 stars in the RC feature detected in all three bands, JHK_s, of the GALACTICNUCLEUS survey, superseding our previous study by a factor ~3 (Nogueras-Lara et al. 2019b).

We confirmed the wavelength dependence of the extinction curve in the NIR and derived values of $\alpha_{JH} = 2.44 \pm 0.05$ and $\alpha_{HK_s} = 2.23 \pm 0.05$, combining the results for different regions and methods. Thus, we estimated that the difference between both extinction indices is $\Delta\alpha = 0.21 \pm 0.07$, where the uncertainties were quadratically propagated. These values are compatible

Table 3. Results compared with Hosek et al. (2018).

Parameter	This work	Hosek et al. (2018)
A_J/A_{K_s}	3.44 ± 0.08	3.52 ± 0.03
A_H/A_{K_s}	1.84 ± 0.03	2.01 ± 0.05
α_{JH}	2.44 ± 0.05	2.17 ± 0.07
α_{HK_s}	2.23 ± 0.05	2.56 ± 0.04

Notes. We computed the values from Hosek et al. (2018) using the code that they made publicly available (`http://faun.rc.fas.harvard.edu/eschlafly/apored/extcurve_s16.py`) and computed the uncertainties quadratically propagating the obtained statistical uncertainties.

with the previous results ($\alpha_{JH} = 2.43 \pm 0.03$ and $\alpha_{HK_s} = 2.23 \pm 0.03$) obtained by Nogueras-Lara et al. (2019b). The uncertainties of the new results are somewhat higher due to the larger size of the sample and the combination of values belonging to different regions or obtained by using independent methods. Our study confirms the evidence of a wavelength dependence also pointed out by Nogueras-Lara et al. (2018a) and Hosek et al. (2018).

These new results might solve the apparent disagreement between the extinction indices obtained by independent groups that computed a single α for the NIR bands JHK_s (e.g. Nishiyama et al. 2006; Stead & Hoare 2009; Gosling et al. 2009; Fritz et al. 2011; Alonso-García et al. 2017; Deno Stelter & Eikenberry 2020). Moreover, using our results to correct the photometry from distance estimators might lead to a change in the picture of the inner regions of the Milky Way (e.g. Matsunaga et al. 2016). Namely, a variation of ∼10−15% in the extinction index might produce a change of ∼0.3 mag in absolute extinction that would lead to a biased distance calculation of around ∼1000 pc for the GC distance, when using RC stars and the distance modulus for the estimation.

To compare our results with the extinction curve obtained by Hosek et al. (2018), we computed the extinction ratios A_J/A_{K_s} and A_H/A_{K_s} using the effective wavelengths that we calculated for the central region of the GALACTICNUCLEUS survey (considering $A_{1.61} = 3.40$ mag and the extinction indices that we derived). Table 3 shows the obtained results. The A_J/A_{K_s} values agree within the uncertainties, while the A_H/A_{K_s} ones are different. To analyse this disagreement, we computed the equivalent extinction indices α_{JH} and α_{HK_s} using the Table 5 from Hosek et al. (2018) and the following equation:

$$\alpha_{\lambda_1\lambda_2} = \frac{\log(A_{\lambda_1}/A_{\lambda_2})}{\log(\lambda_1/\lambda_2)}, \quad (3)$$

where A_{λ_i} refers to the extinction at a given wavelength λ_i. We obtained $\alpha_{JH} = 2.17 \pm 0.07$ and $\alpha_{HK_s} = 2.56 \pm 0.04$, where the uncertainties were quadratically propagated using the statistical uncertainties in Table 3. In spite of being two different extinction indices, they show an inverted tendency with respect to our results. Comparing this result with previous works, we found that the vast majority of studies show a tendency that is compatible with our findings. In particular, Fig. 7 from Nishiyama et al. (2009) and Fig. 8 from Fritz et al. (2011) summarise a variety of studies (e.g. Rieke & Lebofsky 1985; Lutz 1999; Indebetouw et al. 2005) that point towards a non-inverted tendency when moving towards redder wavelengths, which is in agreement to our results. Only the values obtained using hydrogen lines by Fritz et al. (2011) might present some evidence of inversion (see Fig. 8 from Fritz et al. 2011), but the final value is compatible with a single extinction index of $\alpha = 2.11 \pm 0.06$.

Moreover, we further analysed this disagreement computing the extinction indices α_{JH} and α_{HK_s} using Eq. (3) and the extinction values from Nishiyama et al. (2009) and Schlafly et al. (2016), along with the associated wavelength values that they give in their papers. We obtained $\alpha_{JH} = 2.10$ and $\alpha_{HK_s} = 2.01$, and $\alpha_{JH} = 2.27$ and $\alpha_{HK_s} = 2.24$, respectively. In the case of Schlafly et al. (2016), we used an $R_V = 3.3$ and adapted the extinction curve to our results using $A_H/A_{K_s} = 1.84$ (instead of the value 1.55 that they used). We checked that in spite of its being consistent with a single extinction index, if there is some tendency, it would be in the direction of the wavelength-dependence that we found. On the other hand, the extinction indices computed by Schödel et al. (2010) for $\alpha_{HK_s} = 2.21 \pm 0.24$ and $\alpha_{K_sL'} = 1.34 \pm 0.29$, also support the tendency of a lower extinction index for redder NIR wavelengths. In this way, we believe that maybe a calibration problem might explain the inverted extinction indices tendency obtained by Hosek et al. (2018). Nevertheless, it is important to note that the majority of studies of the NIR extinction curve, including this one, use wide-band filters for their analysis. This implies that they are limited by non-linear photometric effects (for further details see Jones & Hyland 1980; Straižys & Lazauskaitė 2008; Maíz Apellániz et al. 2020). In particular, the extinction affects a star in a different way, depending on its spectral type and the effective wavelength (defined for wide-band filters) that varies depending on the absolute extinction and the type of star. In this work, we mainly used RC stars as reference stars to analyse the extinction, minimising the inclusion of other kind of stars that might contaminate our results. Moreover, we also defined the effective wavelength for the used RC stars independently for each of the regions, considering the appropriate average absolute extinctions as indicated in Table 2. As a future goal, we aim at analysing the extinction curve using narrow band filters that are less affected by these issues and will help to determine the precise behaviour of the extinction curve.

We showed that evidence of the α_{HK_s} dependence as a function of the absolute extinction in Nogueras-Lara et al. (2019b) was not a real effect and it is, rather, due to systematics in the methodology and some degeneracies, such as the mixture of stars that might be located at different distances in the NSD. Thus, after analysing GALACTICNUCLEUS regions whose extinction is significantly different, we conclude that the extinction index does not show any significant variation with the absolute extinction within the estimated uncertainties.

Finally, we also find that the calculated extinction indices, α_{JH} and α_{HK_s}, do not depend on the line-of-sight and can be assumed as constant within the given uncertainties and the analysed regions, which is in agreement with previous works (Nogueras-Lara et al. 2019a; Deno Stelter & Eikenberry 2020). For this analysis, we considered all the fields observed in the GALACTICNUCLEUS survey, except for the NSD W because its low quality impeded this study. In this way, we covered regions that are within one square degree without finding any significant line-of-sight variation.

Acknowledgements. The research leading to these results has received funding from the European Research Council under the European Union's Seventh Framework Programme (FP7/2007-2013) / ERC grant agreement n° [614922]. This work is based on observations made with ESO Telescopes at the La Silla Paranal Observatory under programmes IDs 195.B-0283 and 091.B-0418. We thank the staff of ESO for their great efforts and helpfulness. F.N.-L. and N.N. gratefully acknowledge support by the Deutsche Forschungsgemeinschaft (DFG, German Research Foundation) – Project-ID 138713538 – SFB 881 ("The Milky

Way System", subproject B8). R.S., A.T.G.-C., E.G.-C., and B.S. acknowledge financial support from the State Agency for Research of the Spanish MCIU through the "Center of Excellence Severo Ochoa" award for the Instituto de Astrofísica de Andalucía (SEV-2017-0709). A.T. G.-C., B.S., and R.S. acknowledge financial support from national project PGC2018-095049-B-C21 (MCIU/AEI/FEDER, UE). F.N. acknowledges financial support through Spanish grant ESP2017-86582-C4-1-R (MINECO/FEDER) and from the Spanish State Research Agency (AEI) through the Unidad de Excelencia "María de Maeztu" -Centro de Astrobiología (CSIC-INTA) project No. MDM-2017-0737.

References

Akaike, H. 1974, IEEE Trans. Auto. Control, 19, 716
Alonso-García, J., Minniti, D., Catelan, M., et al. 2017, ApJ, 849, L13
Blum, R. D., Ramírez, S. V., Sellgren, K., & Olsen, K. 2003, ApJ, 597, 323
Bovy, J., Nidever, D. L., Rix, H.-W., et al. 2014, ApJ, 790, 127
Chaplin, W. J., & Miglio, A. 2013, ARA&A, 51, 353
Deno Stelter, R., & Eikenberry, S. S. 2020, ApJ, submitted
Diolaiti, E., Bendinelli, O., Bonaccini, D., et al. 2000, SPIE Conf. Ser., 4007, 879
Do, T., Hees, A., Ghez, A., et al. 2019, Science, 365, 664
Eisenhauer, F., Quirrenbach, A., Zinnecker, H., & Genzel, R. 1998, ApJ, 498, 278
Feldmeier-Krause, A., Kerzendorf, W., Neumayer, N., et al. 2017, MNRAS, 464, 194
Fritz, T. K., Gillessen, S., Dodds-Eden, K., et al. 2011, ApJ, 737, 73
Gallego-Cano, E., Schödel, R., Nogueras-Lara, F., et al. 2020, A&A, 634, A71
Girardi, L. 2016, ARA&A, 54, 95
Gosling, A. J., Bandyopadhyay, R. M., & Blundell, K. M. 2009, MNRAS, 394, 2247
GRAVITY Collaboration (Abuter, R., et al.) 2018, A&A, 615, L15
Hosek, M. W., Lu, J. R., Anderson, J., et al. 2018, ApJ, 855, 13
Indebetouw, R., Mathis, J. S., Babler, B. L., et al. 2005, ApJ, 619, 931
Jones, T. J., & Hyland, A. R. 1980, MNRAS, 192, 359
Kissler-Patig, M., Pirard, J.-F., Casali, M., et al. 2008, A&A, 491, 941
Kruijssen, J. M. D., Longmore, S. N., Elmegreen, B. G., et al. 2014, MNRAS, 440, 3370
Kurucz, R. L. 1993, VizieR Online Data Catalog: VI/039
Launhardt, R., Zylka, R., & Mezger, P. G. 2002, A&A, 384, 112
Lutz, D. 1999, ESA SP 427, 623
Maíz Apellániz, J., Pantaleoni González, M., Barbá, R. H., García-Lario, P., & Nogueras-Lara, F. 2020, MNRAS, in press [arXiv:2006.09206]
Matsunaga, N., Feast, M. W., Bono, G., et al. 2016, MNRAS, 462, 414
Morris, M., & Serabyn, E. 1996, ARA&A, 34, 645
Nagayama, T., Nagashima, C., Nakajima, Y., et al. 2003, Proc. SPIE, 4841, 459
Neumayer, N., Seth, A., & Boeker, T. 2020, A&ARv, 28, 4
Nishiyama, S., Nagata, T., Kusakabe, N., et al. 2006, ApJ, 638, 839
Nishiyama, S., Nagata, T., Tamura, M., et al. 2008, ApJ, 680, 1174
Nishiyama, S., Tamura, M., Hatano, H., et al. 2009, ApJ, 696, 1407
Nishiyama, S., Yasui, K., Nagata, T., et al. 2013, ApJ, 769, L28
Nogueras-Lara, F., Gallego-Calvente, A. T., Dong, H., et al. 2018a, A&A, 610, A83
Nogueras-Lara, F., Schödel, R., Dong, H., et al. 2018b, A&A, 620, A83
Nogueras-Lara, F., Schödel, R., Gallego-Calvente, A. T., et al. 2019a, A&A, 631, A20
Nogueras-Lara, F., Schödel, R., Najarro, F., et al. 2019b, A&A, 630, L3
Nogueras-Lara, F., Schödel, R., Gallego-Calvente, A. T., et al. 2020, Nat. Astron., 4, 377
Pedregosa, F., Varoquaux, G., Gramfort, A., et al. 2011, J. Mach. Learn. Res., 12, 2825
Pfuhl, O., Fritz, T. K., Zilka, M., et al. 2011, ApJ, 741, 108
Rieke, G. H., & Lebofsky, M. J. 1985, ApJ, 288, 618
Schlafly, E. F., Meisner, A. M., Stutz, A. M., et al. 2016, ApJ, 821, 78
Schödel, R., Najarro, F., Muzic, K., & Eckart, A. 2010, A&A, 511, A18
Schödel, R., Feldmeier, A., Kunneriath, D., et al. 2014, A&A, 566, A47
Schultheis, M., Rich, R. M., Origlia, L., et al. 2019, A&A, 627, A152
Schwarz, G. 1978, Ann. Stat., 6, 461
Stead, J. J., & Hoare, M. G. 2009, MNRAS, 400, 731
Straižys, V., & Lazauskaitė, R. 2008, Bal. Astron., 17, 277
Tokunaga, A. T., & Vacca, W. D. 2005, PASP, 117, 421